Computer Modeling of Selective Regions in the Active Site of Nitric Oxide Synthases: Implication for the Design of Isoform-Selective Inhibitors

Haitao Ji,[†] Huiying Li,[‡] Mack Flinspach,[‡] Thomas L. Poulos,[‡] and Richard B. Silverman*[,†]

Department of Chemistry, Department of Biochemistry, Molecular Biology, and Cell Biology, and the Drug Discovery Program, Northwestern University, Evanston, Illinois 60208-3113, and Department of Molecular Biology & Biochemistry and Physiology & Biophysics and the Program in Macromolecular Structure, University of California, Irvine, California 92697

Received June 19, 2003

Selective inhibition of nitric oxide synthase (NOS) isoforms has great therapeutic potential in the treatment of certain disease states arising from the pathological overproduction of nitric oxide. In this study three structures of each NOS isoform were employed to examine selective regions in the active site using the GRID/CPCA approach. In the GRID calculations, 10 probes covering hydrophobic, steric, and hydrogen-bond-acceptor and -donor interactions were used to calculate the molecular interaction fields (MIFs) in the active site. The side chain flexibility of the residues and the grid spacings were considered at the same time. Consensus principal component analysis (CPCA) was applied to analyze the MIFs differences in the active site between the NOS isoforms. By combining the cutout tool with GRID/CPCA pseudofield differential plots, several selective regions in the active site were identified. The selectivity analysis showed that the most important determinants for NOS inhibitor selectivity are hydrophobic and charge−charge interactions. Twenty-five inhibitors of NOS were then docked into the active site using the program AutoDock3.0. The regions identified as being important for selectivity by this method are in excellent agreement with inhibitor structure−activity relationships. A rational usage of the selective region described in this work should make it possible to develop NOS isoform-selective inhibitors.

Introduction

Nitric oxide synthase (NOS) catalyzes the biosynthesis of nitric oxide (NO) using L-arginine as the substrate.[1] L-Arg is first converted to N^G-hydroxy-L-arginine, and then in a second step N^G-hydroxy-L-arginine is oxidized to L-citrulline and NO.[2] NO contributes to a broad range of physiological functions in diverse cellular processes, including neurotransmission, regulation of blood pressure, and the immune response.[3] Three isoforms of NOS have been identified: neuronal NOS (nNOS),[4,5] endothelial NOS (eNOS),[6,7] and inducible NOS (iNOS).[8,9] The three NOS isoforms share approximately 50% sequence identity and have identical overall architecture. Native NOS is a homodimeric enzyme. Each subunit contains a catalytic N-terminal oxygenase domain, a C-terminal electron-supplying reductase domain, and a calmodulin (CaM)-binding motif linking the two functional domains.[10,11] The oxygenase domain binds heme, tetrahydrobiopterin (H_4B), and L-Arg. The reductase domain binds FAD, FMN, and NADPH. The heme domain provides the site for L-Arg oxidation, while the FAD and FMN of the reductase domain transfer the electrons from NADPH to the heme.[12] Dimerization and H_4B binding are also essential for the catalytic activity.[13−15]

Although similar in their catalytic mechanism, the NOS isoforms are distinguished by their regulation and localization. nNOS and eNOS are expressed constitutively in neurons and endothelial cells, respectively, among other cell types. Their activities are regulated at the posttranslational level, and NO production is completely dependent on Ca^{2+}/CaM binding.[16,17] However, iNOS is only expressed after induction and is located in macrophages. Its activity is controlled at the transcription level and, once expressed, that isoform will produce NO at a high rate. In addition, iNOS is not regulated by CaM, but instead CaM is bound with high affinity and functions as a permanent subunit.[18] Under normal conditions, NO mediates the regulation of blood pressure and cerebral blood flow associated with neuronal activation. Uncontrolled generation of NO, however, can lead to undesirable pathologies. While overproduction of NO by nNOS and iNOS is directly linked to the pathogenesis of stroke and septic shock, respectively, NO generated by eNOS has been shown to be critical for angiogenesis and for maintaining proper vascular tone.[19,20]

Because of the double-edged nature of NO, the development of isoform-specific NOS inhibitors is a highly desirable goal.[21,22] The ideal inhibitors should inhibit NO production by nNOS or iNOS under pathological conditions without interfering with NO generation by eNOS. Considerable effort has been devoted to developing NOS inhibitors. All of the inhibitors described bind to the oxygenase domain of NOS, and most of them interact with the substrate-binding site. These inhibitors are analogues of L-Arg or compounds bearing guanidine, amidino, or isothiourea functional groups that can mimic the binding mode of the guanidine moiety of L-Arg. Some of these inhibitors show signifi-

* Corresponding author. Phone: (847) 491-5653. Fax: (847) 491-7713. E-mail: Agman@chem.northwestern.edu.
[†] Northwestern University.
[‡] University of California.

10.1021/jm030301u CCC: $25.00
Published on Web 11/22/2003

cant isoform selectivity. In addition, some pterin-based analogues also were developed that target the H_4B-binding site. Crystal structures of the oxygenase domain of the three NOS iosforms have been determined, which provides an opportunity to accelerate the development of NOS inhibitors.[23−28] All of these structures, however, showed a striking similarity to each other in overall structural features as well as in the substrate-binding site. Given such close similarity, structure-based isoform-specific inhibitor design presents an especially challenging problem.[26,27]

To circumvent this problem, it is essential to ascertain the structural differences in the active site among the three NOS isoforms and to understand how the known isoform-selective inhibitors interact with the active site. The GRID/CPCA method allows a detailed investigation of structural differences important for selectivity within a given family of target proteins. On the basis of the 3D structures of the proteins, this method analyzes the selectivity differences from the viewpoint of the receptor and is therefore independent of the availability of appropriate ligands for a ligand-based QSAR analysis.[29−31]

In the present study, the active sites of nine NOS structures were characterized by examination of molecular interaction fields (MIFs) obtained by 10 different GRID probes. The differences in MIFs were evaluated by the consensus principal component analysis (CPCA) method. Twenty-five selective NOS inhibitors were then docked into the active site with the program AutoDock3.0.[32] The structural determinants for inhibitor selectivity were identified and are discussed. The selective regions from the analysis transformed into the pharmacophoric map are of particular interest for further NOS inhibitor design.

Materials and Methods

Protein Structures. The amino acid sequences of NOS were retrieved from the PIR protein sequence database. The sequences were human nNOS (entry G01946), rat nNOS (entry P29476), human eNOS (entry P29474), bovine eNOS (entry P29473), human iNOS (entry P35228), and murine iNOS (entry P29477). The crystallographic coordinates of NOS used in this study were taken from in-house X-ray data or from the Research Collaboratory for Structural Bioinformatics (RCSB) protein database.[26,27,33−35] Three structures determined by different research groups were used for each NOS to minimize errors in the crystal structure data and to understand the effect on the analysis of enzymes from different sources. The sequence alignment was performed using the Needleman−Wunsch algorithm implemented in SYBYL/Biopolymer.[36] The permutation homology matrix was used to evaluate amino acid similarity. The gap penalty was 8.

GRID Calculations. The calculations were performed with version 20 of the GRID software.[37] Hydrogens were added with the program GRIN. The GRID box dimensions were chosen to encompass all of the active site residues shown in Figure 1. This results in a box size of 31 × 28 × 31 Å. The grid spacings were set to 1 Å (directive NPLA = 1) and 0.5 Å (directive NPLA = 2), respectively. Two GRID calculations were made: one where the amino acids in the active site were considered rigid (directive move = 0) and another where they were considered flexible (directive move = 1). The directives NETA and ALMD were set to 120 and 1, respectively, to include the atoms of heme and H_4B into calculations and to interpret which atom(s) in the active site contribute(s) to the interaction with a specific probe atom. The following single atom probes were used in the calculation: DRY, C3, NM3, N1+, N1, N:, NH═, O, OH, and the multiatom probe COO^-. Hydrophobic interactions are calculated with the DRY probe. The C3 and NM3 probes describe the steric interactions. N1+, NM3, and COO^- probes are charged. The polar probes consist of N1, N:, NH═, O, and OH.

CPCA Analysis. The molecular interaction fields (MIFs) from the GRID calculations were imported into the GOLPE program, version 4.5.12.[38] A maximum cutoff was set to 0 kcal/mol to consider only the favorable protein−ligand interactions (negative energy values). The positive interaction energy is in most cases due to unfavorable steric repulsions between the probes and the atoms in the box. Because the equations used for calculations of the MIFs values are very different for the different probes, block unscaled weights (BUW) were used to normalize the interaction energies between the different probes so as to make sure that each probe would get the same importance in the model. Variables with values smaller than 0.01 kcal/mol and those with a standard deviation below 0.02 were removed to eliminate noisy variables. The analysis was made in both the originally defined box volume (31 × 28 × 31 Å) and on a limited region defined by a given fragment encompassing all of the atoms of the specific pocket of the active site using the cutout tool. This allows focusing on the region of interest, while the regions not important could be left out of the calculation.

The pretreated data were then used in CPCA modeling. CPCA is one of the hierarchical principal component analysis (PCA) methods, which captures the information both in each block (i.e., probes) and from the whole X-matrix (i.e., MIFs values).[39] Compared to PCA, the advantage of CPCA is that this analysis allows the investigation of more than two enzymes and can be regarded as a PCA at two different levels: one is the block level, which provides the relative importance of the different probes; another is the superlevel, which is a combination of these blocks to yield an analysis for the overall data (results are similar to the results from the usual PCA). Each of these levels has loading and score vectors that summarize the information like in a usual PCA, but they are called CPCA loading and score plots, respectively. However, in a selectivity study often more than one principal component contributes to discriminate different objects in the scores plot, and therefore, any single CPCA loadings plot can only partially describe the MIFs difference for a specific GRID probe between different target proteins. By using active CPCA differential plots implemented in the GOLPE program, the difference between the two points for the first and second principal component can be calculated and projected back into the original space (a pseudofield) using PCA loading. That is, the vector linking pairs of objects in a 2D score plot can be translated into isocontour plots that identify those variables that contribute most to differentiate the selected objects.[29] On the other hand, the use of the cutout tool of GLOPE facilitates the identification of probes that can distinguish between the different target enzymes within a selected region.

Docking Analysis. AutoDock3.0 was employed to perform the docking calculations. The protein structures used in the docking studies were nNOS and eNOS in complex with L-NNA,[26] and iNOS in complex with L-Arg.[27] The ligands and solvent molecules were removed, but the heme and H_4B were retained near the active site. For each protein structure, polar hydrogen atoms were added, and Kollman united atom charges were assigned.[40] Hydrogens were also added to the heme and H_4B, and charges were calculated by the Gasteiger−Marsili method.[41] The Fe atom of heme was assigned a charge of +3. The nonpolar hydrogen atoms were then removed manually and their charges were united with the bonded carbon atoms. Atomic solvation parameters and fragmental volumes were assigned using the AddSol utility of AutoDock3.0. The 3D structures of the ligands were built using the molecular modeling program SYBYL. The ligands were treated in SYBYL initially as all atom entities, i.e., all the hydrogens were added. Partial atomic charges were also calculated using the Gasteiger−Marsili method. The rotatable bonds in the ligands were defined using another AutoDock3.0 auxiliary program,

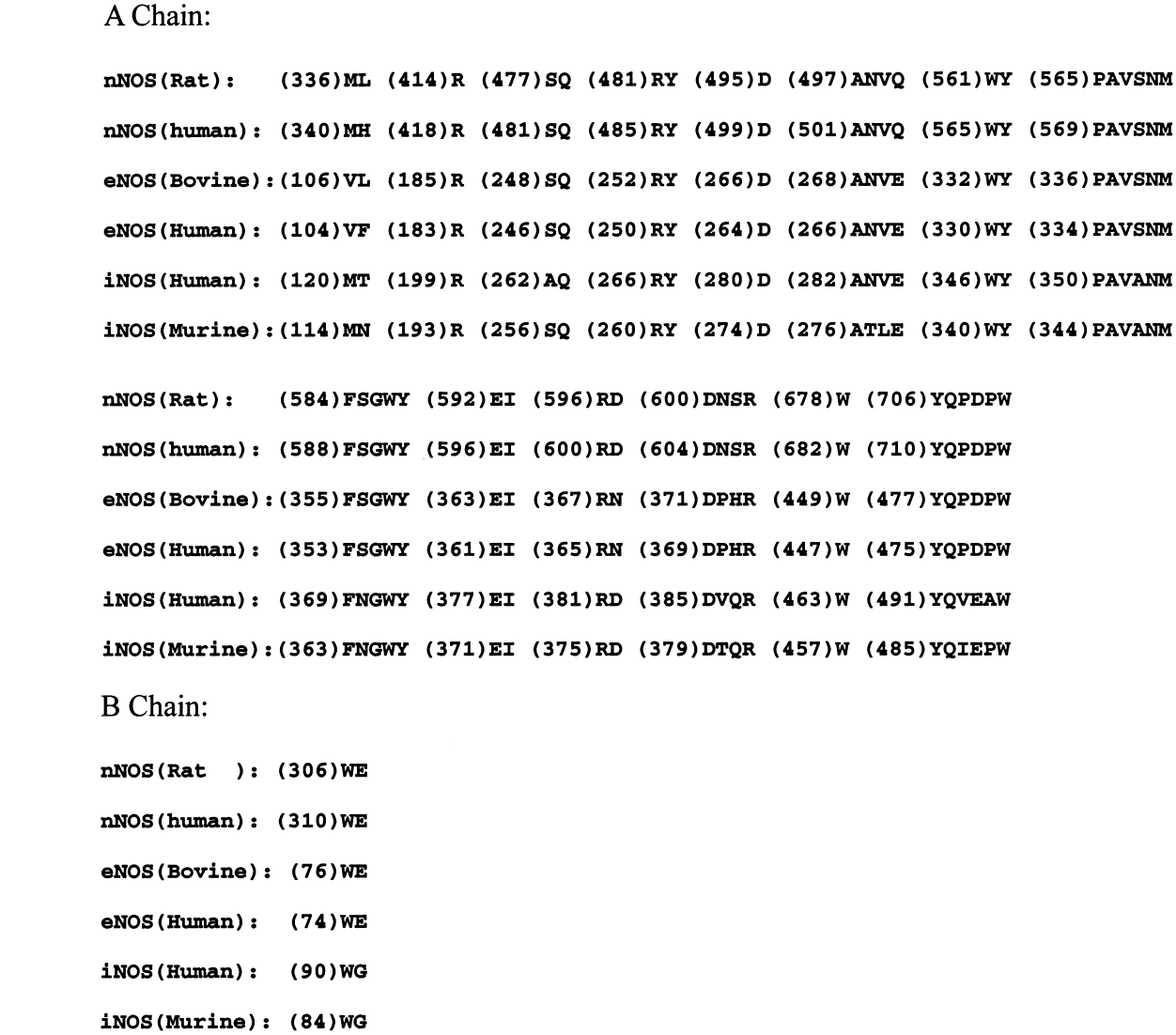

Figure 1. Sequence alignment for the active site of NOS.

AutoTors, which also unites the nonpolar hydrogens and partial atomic charges to the bonded carbon atoms.

The grid maps were calculated using AutoGrid. As was used in the GRID calculations, the dimensions of the grid box was 31 × 28 × 31 Å, but the grid spacing was set to 0.375 Å. Lennard-Jones parameters 12−10 and 12−6 were used for modeling H-bonds and van der Waals interactions, respectively.[32,42] The distance-dependent dielectric function was used for the calculation of the electrostatic grid map. Docking was performed using the Lamarckian genetic algorithm (LGA), and the pseudo-Solis and Wets methods were applied for the local search. Each docking experiment was performed 100 times, yielding 100 docked conformations. Parameters for the docking experiments were as follows: initial population size of 200, random starting position and conformation, maximal mutation of 0.2 Å in translation and 5° in orientation and rotation, elitism of 5; mutation rate of 0.02, crossover rate of 0.8, local search rate of 0.06, and maximal iteration per local search of 300. Simulations were performed with a maximum of 1.5×10^6 energy evaluations and a maximum of 27 000 generations. All of the ligands followed the same docking protocol. The results of the docking experiments were evaluated by calculating the positional root-mean-square (rms) deviation of the corresponding atoms of each conformation.[43] The clustering tolerance was set to 2 Å. The ligand conformation with the lowest energy in each class was then used for the analysis of its interaction mode with the active site.

Table 1. Protein Structures Used in the GRID/CPCA Analysis

enzyme	ligand	organism	PDB entry	resolution	rms deviation
nNOS	L-NNA	rat	1k2r	2.15	0
nNOS	L-PLA	rat	1mmv	2.00	0.225
nNOS	L-ALA	rat	1k2s	2.55	0.205
eNOS	L-NNA	bovine	8nse	2.25	0.771
eNOS	SENPITU	bovine	1d1v	1.93	0.790
eNOS	L-Arg	human	3nos	2.40	0.729
iNOS	L-Arg	human	1nsi	2.55	0.775
iNOS	SEITU	human	4nos	2.25	0.890
iNOS	L-NHA	murine	1dww	2.35	0.809

Results and Discussion

1. The Active Site of NOS. Table 1 lists the crystal structures used in this study. Crystallographic structures for all of the three isoforms show a similar active site. Figure 1 shows the multiple sequence alignment of the residues in the active site. The nine NOS crystal structures were superimposed by aligning the backbone atoms in the active site and all of the heavy atoms of the identical residues in the active site. The rms deviations for the superpositions are listed in Table 1. In the following discussion, the residue numbering of rat nNOS, bovine eNOS, and human iNOS are used for each isoform. The unconserved residue within the

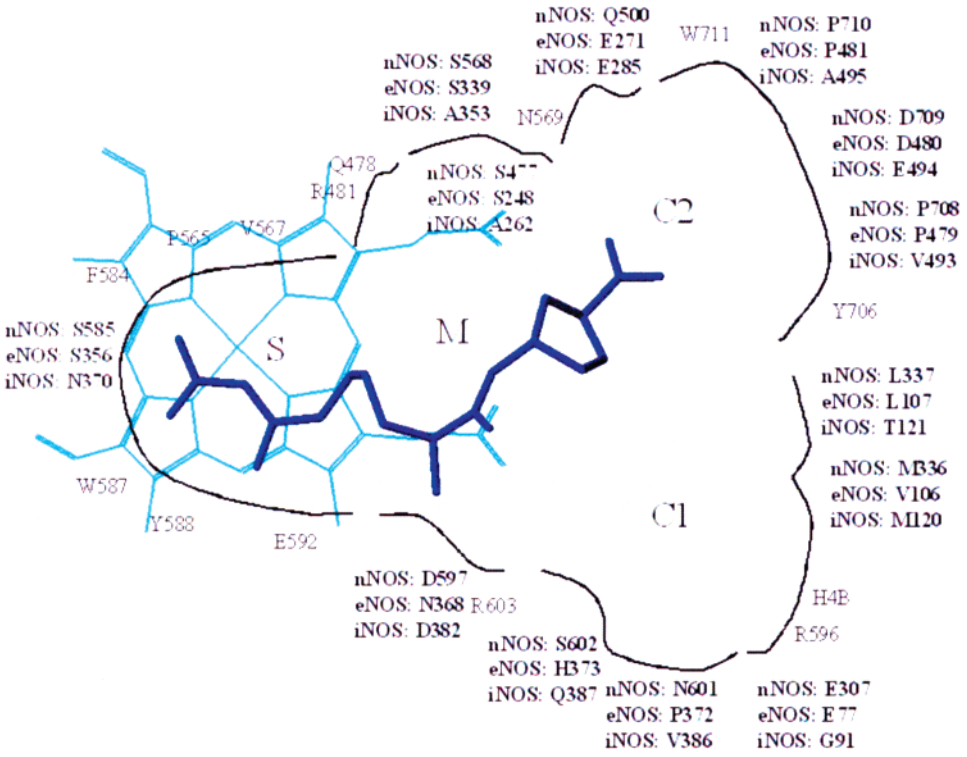

Figure 2. Schematic drawing of the active site of NOS. The binding mode of **IV-1** is shown to indicate the S, M, C1, and C2 pockets. Amino acids important for inhibitor binding are indicated. Numbering is according to the sequence of rat nNOS. Residues that differ between NOS are highlighted.

isoform that is important for human enzymes also is highlighted. The bottom of the active site is defined by heme, H_4B, helix H15 (nNOS W678), and the loop between helix H5 and H6 (nNOS R414). The numbering of the secondary structure of NOS follows the nomenclature of Fischmann et al.[26] The active site is bordered on the side by the loop between helix H1 and H2 (nNOS M336-L337), β-sheet S12 (nNOS P565-M570), the N-terminus of helix H11 (nNOS F584-Y588, E592-I593, R596-D597), the loop between β-sheet S18 and helix H18 (nNOS Y706-D709), and two residues from another monomer (nNOS W306-E307). The top of the active site consists of the loop between β-sheet S5 and S6 (nNOS S477-Q478, R481-Y482), the N-terminus of helix H8 (nNOS D485, A497-Q500), β-sheet S11 (nNOS W561-Y563), the loop between helix H11 and H12 (nNOS D600-R603), and two residues from helix H18 (nNOS P710-W711). Figure 2 shows a schematic drawing of the active site of NOS with the amino acids highlighted that differ among the three isoforms. The active site of NOS can be divided into four pockets. The S pocket is above the heme ring, which is the catalytic site for the substrate L-Arg. All of the residues in this pocket are identical, except for S585 in nNOS, which is N370 in iNOS. Most parts of the substrate L-Arg were located in this pocket. The guanidino group of the substrate and the gaunidino, amidino, or isothioureido groups of inhibitors form two syn hydrogen bonds with the side chain carboxylate of conserved residue Glu592 and one hydrogen bond with the carbonyl group of Trp587.[44] The α-amino group of the substrate also forms a hydrogen bond with this conserved glutamate. One hydrophobic patch is located in the S pocket, which is composed of the side chain of F584, V567, and P565.[45]

The M pocket is in the middle of the substrate catalytic site and the substrate access channel. Three residues in this pocket are different among the NOS isoforms. One is D597 of nNOS, which is N368 in eNOS. The other two are S477 and S568 of nNOS, which are A262 and A353 in iNOS. In the M pocket there are also some conserved polar/charged residues that play an important role in substrate and inhibitor binding, such as Q478, R481, N569, and R603 of nNOS (Figure 2).

The C1 and C2 pockets are slightly away from the

Table 2. Overview of the Probes Used in the GRID Calculation

probe	chemical group	charges	no. of H bonds	
			accepted	donated
DRY	hydrophobic probe	0	0	0
C3	methyl group	0	0	0
NM3	trimethylammonium cation	1	0	0
N1+	sp^3 amine NH cation	1	0	1
COO^-	carboxylic acid anion	−1	2	0
N1	neutral flat NH (e.g. amide)	0	0	1
N:	sp3 N with lone pair	0	1	0
NH=	sp2 NH with lone pair	0	1	1
O	sp2 carbonyl oxygen	0	2	0
OH	phenol or carboxy OH	0	1	1

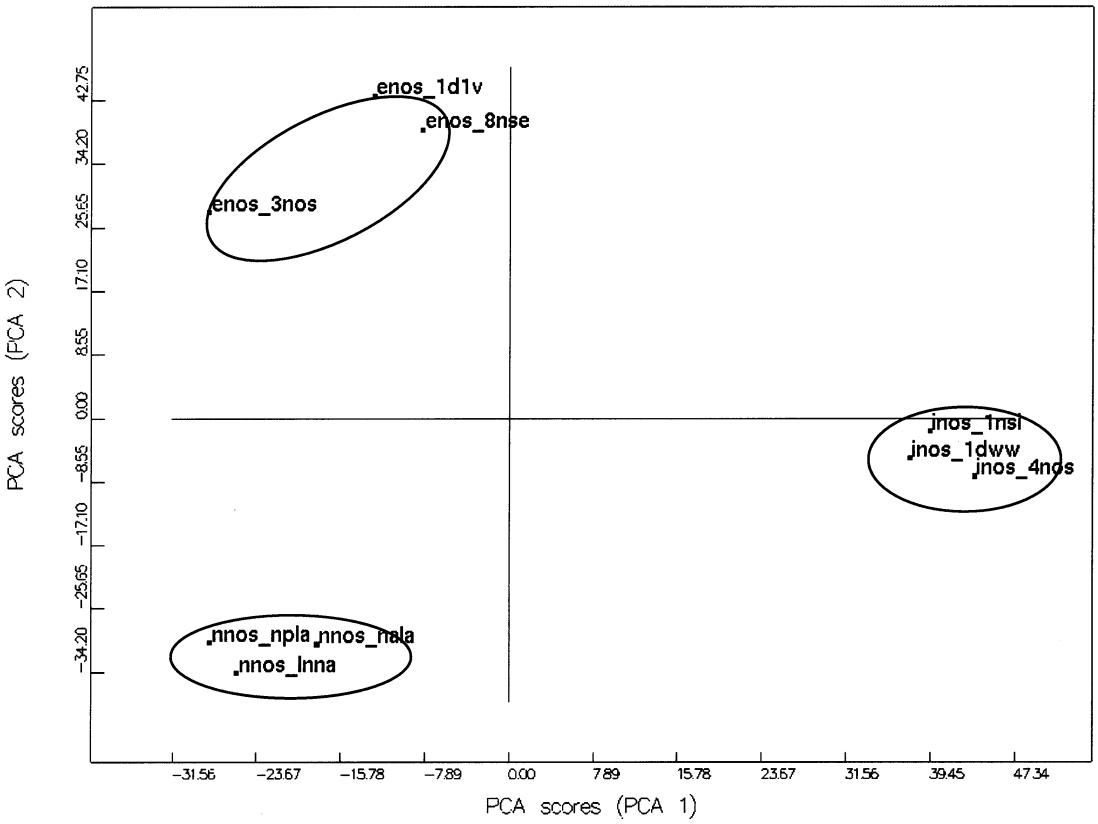

Figure 3. CPCA score plot for the N1+ probe. The clustering of the various structures for each isoform used in the analysis is evident. PC1 can be used to discriminate iNOS from eNOS and nNOS, whereas PC2 discriminates between eNOS and the other two NOS isoforms.

substrate-binding cavity. They constitute the substrate access channel.[34] In these two pockets there are more residues different among the NOS isoforms, as shown in Figure 2. M336 and L337 of nNOS are located at the entrance of the C1 pocket. L337 is T121 in iNOS, and M336 is V106 in eNOS. E307, N601, and S602 of nNOS on the dome of the C1 pocket are also other residues in eNOS and iNOS. In the C2 pocket, P708, D709, and P710 of nNOS is V493, E494, and A495 in iNOS, while Q500 of nNOS is E271 of eNOS and E285 of iNOS, respectively. Some exposed polar/charged residues and the functional groups of the cofactor in these two pockets can also form strong hydrogen bonds with the ligands, such as R596, Y706, and the carbonyl group of the H_4B.

2. Identification of the Selective Regions with the Probe Atoms. The NOS 3D structures were evaluated with emphasis on differences as expressed by the interaction energies with the different GRID probes. A short description of the used probes and their ability to form hydrogen bonds are described in Table 2. The interpretation of the MIFs became more straightforward by translation of the CPCA loadings into the contour plots. Changing the distance between grid points from 1 to 0.5 Å had no significant effect on the result, but increased the computational consumption dramatically. Some MIFs differences were also found in the contour plot near the conserved residues, such as R481, N569, and W711 of nNOS, which results from the slight differences in the side chain conformations of these residues for the different NOS isoforms. When incorporating the side chain conformation flexibility (directive MOVE = 1) in the calculation, the MIFs differences caused by these conserved residues disappeared, while the MIFs differences caused by the selective residues in the active site were still apparent. As identified from the score plots shown in Figure 3, the differences between the 3D structures of the same isoforms are less important than those between the NOS isoforms. The first component in all of the analyses discriminates between iNOS and the other two enzymes, whereas the second component discriminates between eNOS and the rest of the NOS enzymes. Below, each pocket in the active site is described individually.

S Pocket. With the exception of the N370S mutation in iNOS (Figure 2), the S pockets are identical in all three NOS isoforms. Because the side chain of this residue points outside of the active site, and both Asn and Ser are uncharged polar residues, there are no pronounced differences in the CPCA pseudofield differential contour plots for all 10 probes. This means that it is difficult to explain why some L-Arg analogues, such as L-VNIO (K_i values for nNOS = 0.10 μM, eNOS = 12.0 μM), L-NNA (K_i values for iNOS = 0.015 μM, nNOS = 4.4 μM), and L-NPA (K_i values for nNOS = 0.11 μM, eNOS = 10 μM), show selectivity if only the binding of these inhibitors with the residues in the S pocket is considered.[46−48,51]

M Pocket. In contrast to the result for the S pocket, several probes have particularly high interaction energies for one of the isoforms. For the DRY probe, the highest interaction energy (after BUM scaling) of iNOS (E = −36.70 kcal/mol) is much higher than those of nNOS (E = −6.49 kcal/mol) and eNOS (E = −12.03 kcal/mol). For the N1+ probe, the highest interaction energies for nNOS (E = −12.03 kcal/mol) and iNOS (E = −12.68 kcal/mol) are higher than that of eNOS (E =

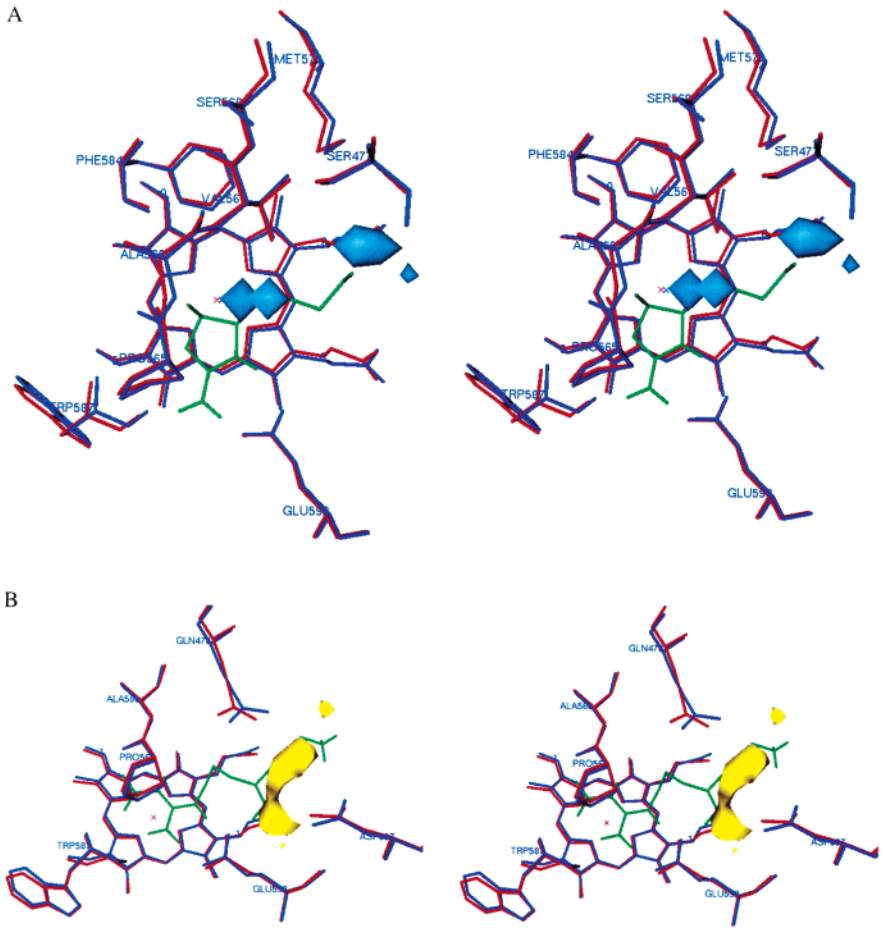

Figure 4. Stereoview CPCA pseudofield plots within the M pocket. (A) shows the field difference of the DRY probe between nNOS (blue) and iNOS (red). Cyan contours indicate regions where interaction energies are more favorable for iNOS. The docking result of **VII-2** (green) is included for illustrative purposes. (B) shows the field difference of the N1+ probe between nNOS (blue) and eNOS (red). Yellow contours indicate regions where interaction energies are more favorable for nNOS. The docking conformation of the **II-3** (green) is included for illustrative purposes.

−7.67 kcal/mol). Therefore, a ligand with a hydrophobic functional group in this region should improve selectivity toward iNOS, while introduction of a positively charged functional group in this pocket should be unfavorable for eNOS. Figure 4a shows the CPCA differential plot between nNOS and iNOS for the DRY probe. Three cyan contours around residues V567, S568, and S477 of nNOS indicate that the introduction of hydrophobic groups in the potential ligand at that position would increase its selectivity for iNOS. The pseudofield differential plot between eNOS and iNOS gave a similar result as that in Figure 4a. (data not shown). Figure 4b shows the pseudofield difference for the GRID N1+ probe between nNOS and eNOS. The large yellow contour around residue D597 of nNOS indicates a region where the interaction between the N1+ probe and this residue is more favorable in nNOS than in eNOS. A very similar contour plot was also obtained if eNOS and iNOS were compared. These results underline the importance of the M pocket in the design of isoform-selective inhibitors.

C1 Pocket. As mentioned above, five residues in this pocket are different among the NOS isoforms. The energy distributions for several GRID probes also showed a difference. For the DRY probe, the highest interaction energies of nNOS ($E = -39.12$ kcal/mol) and eNOS ($E = -36.02$ kcal/mol) are higher than that of iNOS ($E = -26.26$ kcal/mol). Figure 5a shows the pseudofield difference between nNOS and iNOS. The large yellow contour around residue L337 of nNOS indicates that the energy difference is caused by the difference in the hydrophobic residues of nNOS compared with the hydrophilic polar residue (T121) of iNOS. All of the crystal structures of nNOS, however, come from rat brain in this GRID/CPCA analysis. The corresponding residue in human nNOS is histidine. This suggests that the hydrophobicity at this position seems less important for selectivity of human nNOS vs human iNOS. But the chemical properties of histidine are also different from those of threonine and phenylalanine. This residue still can be utilized to design specific inhibitors of human nNOS. For both steric C3 and NM3 probes, the highest interaction energies are found in the nNOS C1 pocket (data not shown). Figure 5b shows the CPCA pseudofield difference between nNOS and eNOS. The yellow contour is around residue S602 of nNOS. This is because the side chain of S602 is shorter than the corresponding residues in eNOS and iNOS and leads to an extra pocket in the active site bordered by S602, N601, and E307 (from another monomer). The cyan contour favorable for eNOS in Figure 5b is caused by the difference between nNOS M336 and eNOS V106. The cationic N1+ probe showed the highest energies for nNOS ($E = -13.11$ kcal/mol), higher than that for iNOS ($E = -9.86$ kcal/mol). This is because of the difference between E307 in nNOS and G91 in iNOS in the extra

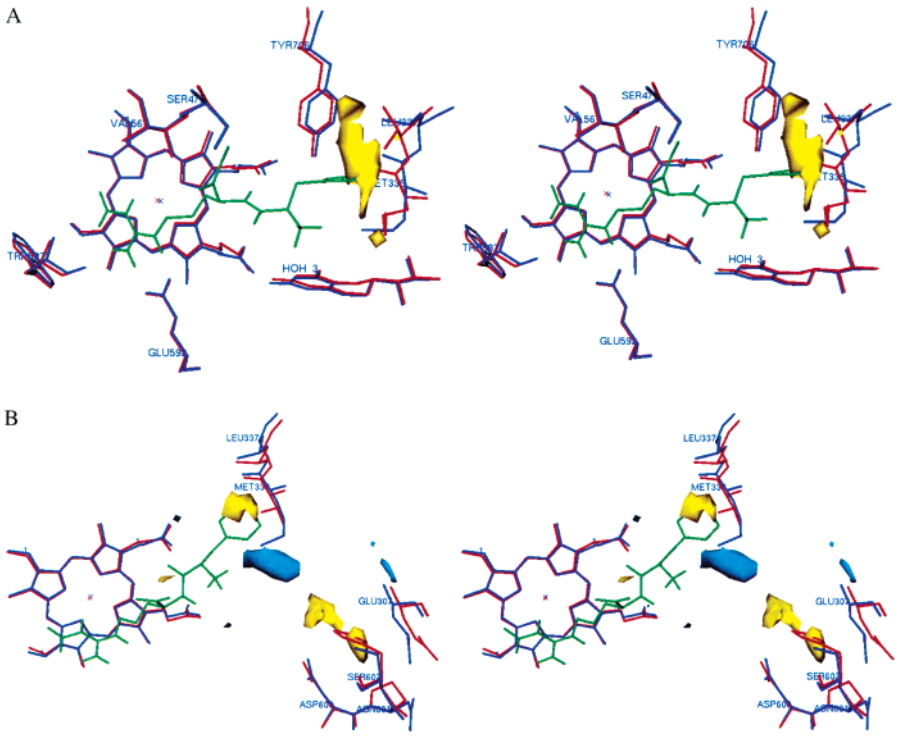

Figure 5. Stereoview CPCA pseudofield plots within the C1 pocket. (A) shows the field difference of the DRY probe between nNOS (blue) and iNOS (red). Yellow contours indicate regions where interaction energies are more favorable for nNOS. The docking result of **VI-2** (green) is included for illustrative purposes. (B) shows the field difference of the C3 probe between nNOS (blue) and eNOS (red). Yellow contours indicate regions where interaction energies are more favorable for nNOS. Cyan contours indicate regions where interaction energies are more favorable for eNOS. The docking result of **VI-1** (green) is included for illustrative purposes.

pocket, as identified from the pseudofield differential plot (data not shown). Although the distance between the Cα atom of E307 and the Fe atom of heme is 21.99 Å, the distance between this Cα atom and the N5 atom of H_4B is only 9.67 Å, suggesting that it is possible to utilize this extra pocket to design nNOS-selective pterin antagonists.[49]

C2 Pocket. There are four residues in this pocket that are different among the NOS isoforms, but two residues (Q500 and P708 of nNOS) point outside the active site. For the C3 probe, the calculated interaction energy for iNOS ($E = -12.57$ kcal/mol) is higher than those for nNOS ($E = -9.29$ kcal/mol) and eNOS ($E = -9.41$ kcal/mol). The CPCA pseudofield differential plot shows that the difference in energy is caused by the difference between the nNOS P710 and the iNOS A495, which makes the volume for the C2 pocket of iNOS larger. The orientation of the side chain carboxylate of the nNOS D709 is different from that of the iNOS E494. The side chain carboxylate of iNOS E494 points toward the solvent outside the active site. Figure 6 shows the CPCA pseudodifference field plot between nNOS and iNOS for the cationic N1+ and NM3 probes. The large yellow contour around residue D709 of nNOS indicates that inhibitors with a positively charged functional group at this position should be favorable for selectivity toward nNOS.

3. Selectivity of the Known Inhibitors. Several known NOS inhibitors shown in Figure 7 were docked into the active site by AutoDock3.0 to understand the relevance of the selective regions that were identified.[50−57] To evaluate the effectiveness of the AutoDock3.0 technique in the flexible docking of NOS ligands, nine different NOS−substrate/inhibitor complexes in Table 1 were chosen as test cases. Using the Lamarckian genetic algorithm and the parameters listed in Materials and Methods, all of the observed crystallographic conformations can be reproduced by the docking experiments. Because of the resolution limits of the crystallographic structure, the location of the ideal positions of the atoms of the protein and the ligand could not be located. This causes bond disharmony and bad bumps between the receptor and the ligand, and the binding energies of the docked conformations are lower than those of the crystallographic molecular conformations.

We previously reported nitroarginine-containing dipeptide amides and some peptidomimetic analogues as selective inhibitors of nNOS.[50−55] Excellent inhibitory potency and selectivity for nNOS over eNOS and iNOS were achieved. **I-3**, **II-3**, **III-2**, and **IV-1** exhibit high selectivity over eNOS (Figure 7). From the docking results, the common α-amino group of these inhibitors is located in the selective region defined by nNOS D597/eNOS N368 in the M pocket. The same binding conformations for **I-3**, **II-3**, and **IV-1** in nNOS were observed from the crystal structures.[58] Figure 4b shows that the α-amino group of **II-3** occupies the same region as the yellow contour, thus contributing to **II-3**'s selectivity for nNOS. The crystal structures of eNOS complexed with **I-3**, **II-3**, and **IV-1** show that the α-amino group is moved away from this selective region, which confirms the importance of nNOS D597/eNOS N368 for selectivity.[58] All of the other parts of these molecules interacted with the conserved residues in the active site, and no other parts of the molecules dropped into the selective region as identified by the GRID/CPCA analysis. For

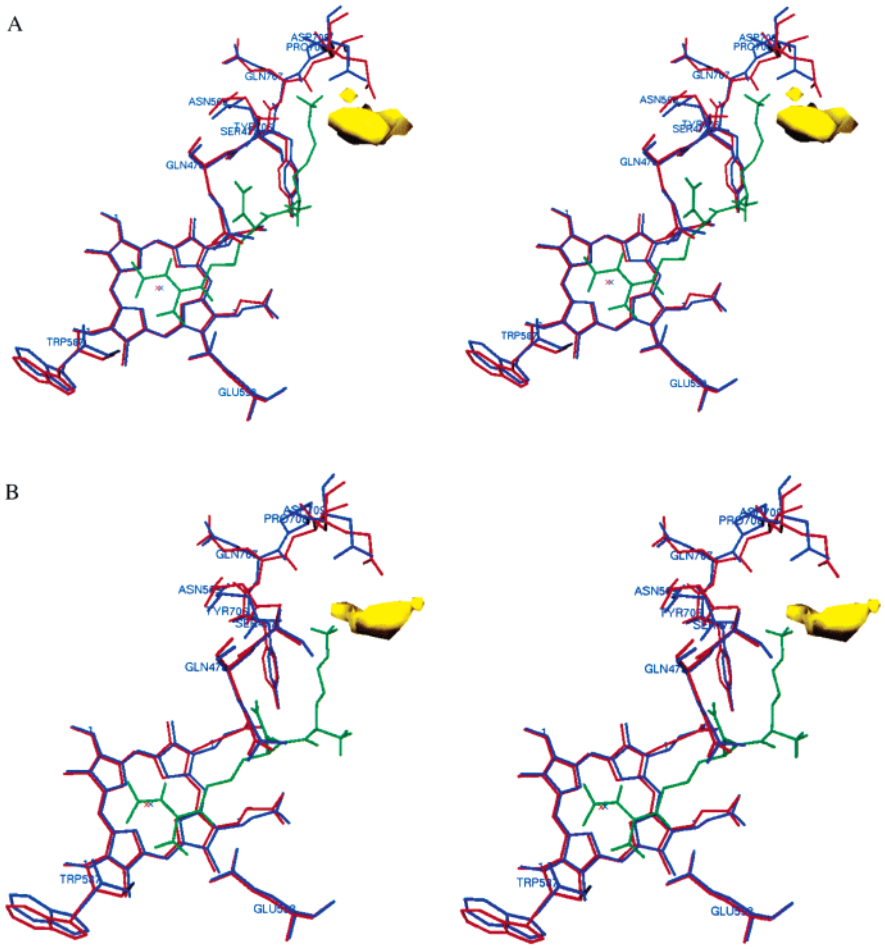

Figure 6. Stereoview CPCA pseudofield plots within the C2 pocket. (A) shows the field difference of the N1+ probe between nNOS (blue) and iNOS (red). The docking conformation of **VI-6** is included for illustrative purposes. (B) shows the field difference of the NM3 probe between nNOS (blue) and iNOS (red). Yellow contours indicate regions where interaction energies are more favorable for nNOS. The docking conformation of **VI-5** is included for illustrative purposes.

example, from the crystal structure (PDB entry 1p6j), the side chain of **IV-1** interacts either directly or through structural waters with the side chain of the conserved residues Q478, R481, Y588, R603, and Y706; the propionate of heme; and the carbonyl group of H_4B.[58] It appears that only the α-amino group of these inhibitors is responsible for the nNOS/eNOS selectivity. However, an interesting phenomenon is that L-NNA also contains an α-amino group, but it exhibits no selectivity between nNOS and eNOS.[44] A comparison of the docking results of **II-3** and L-NNA or the crystal structures of nNOS in complex with **II-3** and L-NNA shows the different orientations of the α-amino groups of **II-3** and L-NNA. As shown in Figure 8, the α-amino group of L-NNA is bent down and forms two hydrogen bonds with the side chain carboxylate of Glu592 and the heme propionate of the pyrrole A ring. This α-amino group is not located in the selective region defined by nNOS D597/eNOS N368 and escapes from the influence of the selective residue nNOS D597/eNOS N368. On the contrary, the α-amino group of **II-3** only forms one hydrogen bond with Glu592 and no hydrogen bonds with the heme propionate. This means that the side chains of **I-3**, **II-3**, **III-2**, and **IV-1** prevent the α-amino group from bending down but fix the α-amino group in the selective region identified above. So, if the side chains of the inhibitors form strong interactions with the residues in the active site, their α-amino group will be more prone to fix at the above selective region in nNOS. That is to say, the derivatives of **I-3**, **II-3**, **III-2**, and **IV-1** with higher potency should exhibit higher selectivity, as is shown in Figure 7. The docking energies of these compounds show that the compound with higher potency forms stronger interactions with the active site.

After this computational work was done, the crystal structure of the nNOS D597N mutant in complex with **I-3** was solved.[58] The binding conformation of **I-3** in nNOS D597N was totally reversed into the binding conformation of **I-3** in wild type eNOS. That provided the crystallographic evidence that the residue nNOS D597/eNOS N368 is the only amino acid responsible for the nNOS selectivity of **I-1**, **II-3**, **III-2**, and **IV-1** relative to eNOS.

Other interesting compounds are **V-1** and **V-2**. **V-1** exhibits more selectivity over eNOS, while **V-2** shows more selectivity over iNOS. The docking model for **V-1** shows that the imino group and the pyridine ring on the side chain form hydrogen bonds with the heme propionate and the conserved residue nNOS N569. This forces the α-amino group of the inhibitor to locate into the selective region discussed above and results in selectivity toward nNOS vs eNOS. When an additional methylene group is added between the pyridine ring and the imino group (**V-2**), the hydrophilic pyridine ring

I.

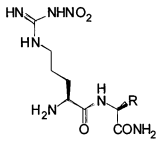

No.	R	Ki (uM) nNOS	eNOS	iNOS	Selectivity n/e	n./i	E_{docked}[a] (Kcal/mol)
I-1		0.45	141	104	313	231	-11.06
I-2		0.33	245	97	742	294	-11.17
I-3		0.13	200	25	1538	192	-11.36
I-4		1.1	261	61	237	55	-10.21

a. The crystallographic coordinates of the receptor is nNOS in complex with L-NNA

II.

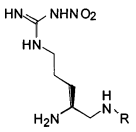

No.	R	Ki (uM) nNOS	eNOS	iNOS	Selectivity n/e	n./i	E_{docked}[a] (Kcal/mol)
II-1	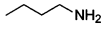	0.46	411	123	898	270	-11.01
II-2		0.29	524	73	1795	250	-11.19
II-3		0.12	314	39	2577	320	-11.34

a. The crystallographic coordinates of the receptor is nNOS in complex with L-NNA

III.

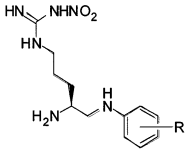

No.	R	Ki (uM) nNOS	eNOS	iNOS	Selectivity n/e	n./i	E_{docked}[a] (Kcal/mol)
III-1	$2\text{-}CH_2NH_2$	5.55	39.8	29.3	7.17	5.28	-10.23
III-2	$2\text{-}CH_2CH_2NH_2$	0.05	105	3.51	2121	70.2	-11.66
III-3	$3\text{-}CH_2NH_2$	0.21	194	80	924	381	-11.11
III-4	$3\text{-}CH_2CH_2NH_2$	2.21	100	260	45.2	118	-10.31
III-5	$4\text{-}CH_2NH_2$	1.37	409	335	299	245	-10.60
III-6	$4\text{-}CH_2CH_2NH_2$	1.66	414	360	249	217	-10.54

a. The crystallographic coordinates of the receptor is nNOS in complex with L-NNA

IV.

No.	R	Ki (uM) nNOS	eNOS	iNOS	Selectivity n/e	n./i	E_{docked}[a] (Kcal/mol)
IV-1	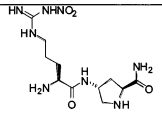	0.074	127.9	29.5	2577	320	-11.94
IV-2	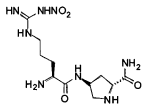	1.10	110	200	100	182	-10.58

a. The crystallographic coordinates of the receptor is nNOS in complex with L-NNA

V.

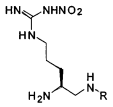

No.	R	Ki (uM) nNOS	eNOS	iNOS	Selectivity n/e	n./i	E_{docked}[a] (Kcal/mol)
V-1		0.55	523	141	951	256	-11.35
V-2		0.76	193	395	254	520	-11.16

a. The crystallographic coordinates of the receptor is nNOS in complex with L-NNA

VI.

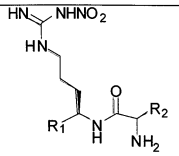

No.	R_1	R_2	Ki (uM) nNOS	eNOS	iNOS	Selectivity n/e	n./i	E_{docked}[a] (Kcal/mol)
VI-1	COOH	(R)-Benzyl	17	90	13600	5.3	800	-9.47
VI-2	$COOCH_3$	(R)-Benzyl	2	5	3600	2.5	1800	-10.36
VI-3	$COOCH_3$	(S)-Benzyl	90	150	7500	1.7	83	-9.13
VI-4	$CONH_2$	(R)-Benzyl	17	90	13600	5.3	800	-9.85
VI-5	$CONH_2$	(R)-$CH_2CH_2CH_2CH_2NH_2$	0.89	30	910	34	1022	-11.19
VI-6	$CONH_2$	(S)-$CH_2CH_2CH_2CH_2NH_2$	1.7	229	4700	135	2765	-10.36

a. The crystallographic coordinates of the receptor is nNOS in complex with L-NNA

VII.

VII-1 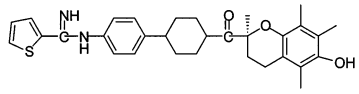 VII-2 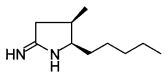

No.	Ki (uM) nNOS	eNOS	iNOS
VII-1	0.92	110	>300
VII-2	3.2	226	0.25

Figure 7. Chemical structures and experimental biological activities of the inhibitors used in the AutoDock calculation and GRID/CPCA analysis.

becomes close to the region surrounded by S477 and S568 of nNOS. In iNOS the corresponding residues are A262 and A353, respectively, which may be responsible for the observed selectivity of **V-2** for nNOS vs iNOS.

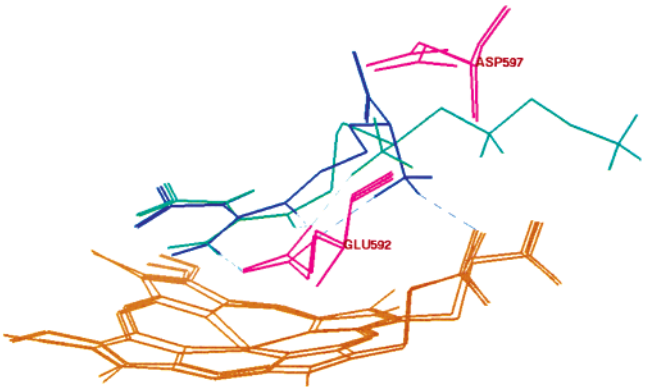

Figure 8. The binding mode of L-NNA (blue) and **II-3** (green) with the active site of NOS, indicating that the orientations of the α-amino groups are different between L-NNA and **II-3**. L-NNA forms two hydrogen bonds with Glu592 and heme propionate, while **II-3** only forms a hydrogen bond with Glu592.

The docking models of compounds **VI-1** to **VI-6** show that the polar R_1 groups located in the selective region defined by residues nNOS S477/iNOS A262 and nNOS S568/iNOS A353 are responsible for the high selectivity of nNOS vs iNOS, as shown in Figure 9. The binding conformations of **VI-4** and **VI-5** observed from the crystal structure are very similar to the docking models. On the other hand, the terminal phenyl rings of **VI-1**, **VI-2**, and **VI-4**, but not the S-isomer **VI-3**, are located in the hydrophobic region defined by M336 and L337 of nNOS. In iNOS the hydrophilic residue T121 occupies the position of nNOS L337, which makes these compounds show higher selectivity toward nNOS relative to iNOS as described in Figure 5a for **VI-2**. Therefore, two determinants make these compounds show selectivity toward nNOS. A similar situation was found for **VI-5** and **VI-6**. From their docking models, the terminal amino groups were close to residue nNOS D709/iNOS E494. Because the side chain carboxylate of iNOS E494 points toward the outside solvent, the yellow contour in Figure 6 rationalizes their nNOS selectivity relative to iNOS.

VII-1 is a selective inhibitor of nNOS vs iNOS. From the docking model, the amide group in the molecule was also located in the selective region defined by nNOS S477/iNOS A262 and nNOS S568/iNOS A353. The polar amide group is more favorable for the polar environment of nNOS. The terminal hydrophobic vitamin E ring is located in the hydrophobic patch defined by M336 and L337 of nNOS. These two determinants make this compound show high selectivity toward nNOS vs iNOS. The hydrophobic alkyl group of **VII-2** also is located in the hydrophobic region defined by A262 and A353 of iNOS, which may be responsible for the selectivity that this molecule shows toward the iNOS isoform (Figure 4a).

Conclusion

The GRID/CPCA approach was used successfully to examine and highlight differences in the NOS isoforms. Especially in the M, C1, and C2 pockets, there are considerable differences among the structures, and these sites are predicted to be very important in the design of selective ligands. In the M pocket, the selective region that was defined by residues nNOS S477/iNOS A262 and nNOS S568/iNOS A353 was responsible for the selectivity of the inhibitors between nNOS and iNOS isoforms. Residue nNOS D579/eNOS N368 is responsible for selectivity of the inhibitor for nNOS over eNOS. In the C1 pocket two selective regions were found, one defined by residues M336 and L337 of nNOS, and another around residues E307, N601, and S602 of nNOS. In the C2 pocket the most important determinant for selectivity is caused by position nNOS D709/iNOS E494. Twenty-five NOS inhibitors were docked into the active site to understand the interaction mode of the inhibitors with the active site and also to understand the importance of the MIFs differences in the active site for the isoform selectivity. The GRID/CPCA pseudofield differential plots rationalized the selectivity difference for the known inhibitors and gave useful insights into key protein−ligand interactions. The present analysis shows that the most important determinants for the selectivity of the NOS inhibitors are hydrophobic and charge−charge interactions. The selectivity of **I**, **II**, **III**, and **IV** for nNOS over eNOS is caused by their common α-amino group, but the side chain also plays an important role in fixing the α-amino

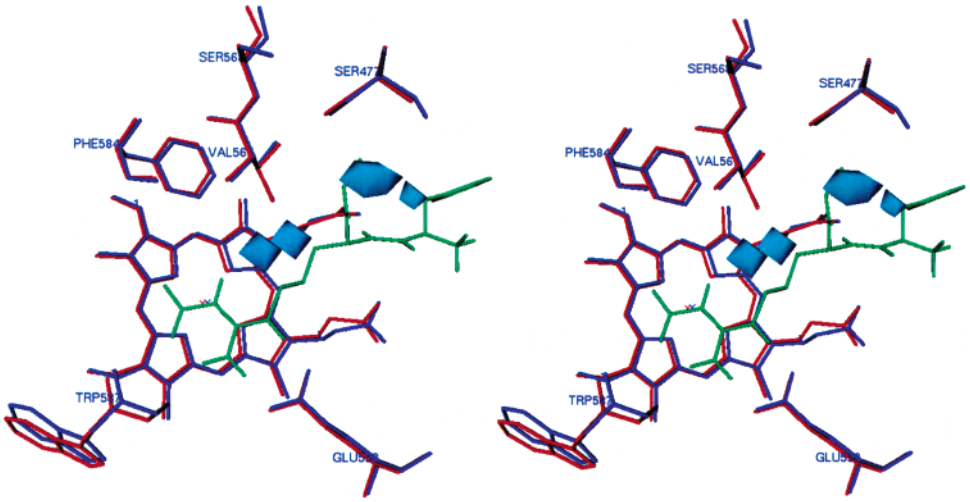

Figure 9. The interaction mode of the R_1 group of **VI** (**VI-2** is shown in the green) with the selective region in the M pocket. A stereoview CPCA pseudofield plot shows the field difference of the DRY probe between nNOS (blue) and iNOS (red). Cyan contours indicate regions where interaction energies are more favorable for iNOS.

group into the selective region. The selectivity of compounds V for nNOS over iNOS is caused by the interaction of their polar R_1 group with the selective regions defined by nNOS S477/iNOS A262 and nNOS S568/iNOS A353. At the same time the terminal phenyl group and the amino group interact with the selective regions in the C1 and C2 pocket, respectively. A rational usage of the findings described in this work provides the opportunity to develop NOS isoform-specific inhibitors. As mentioned above, it was difficult for GRID/CPCA to rationalize the selectivities of L-VNIO, L-NNA, and L-NPA, because few MIF differences were observed in the S pocket for the three NOS isoforms. However, L-VNIO[59] is an inactivator of nNOS, while L-NNA[47] and L-NPA[60] are slow, tight-binding inhibitors of nNOS. These findings suggest that GRID/CPCA is useful for selectivity analysis in the ligand binding step, but it has limited usefulness for selectivity that is caused by a postbinding enzyme kinetics process or enzyme−ligand chemical reaction.

Appendix

Abbreviations: L-ALA, *N*-allyl-L-arginine; L-Arg, L-arginine; CaM, calmodulin; CPCA, consensus principal component analysis; L-NHA, *N*-hydroxy-L-arginine; L-VNIO, N^5-(1-imino-3-butenyl)-L-ornithine; MIFs, molecular interaction fields; NO, nitric oxide; NOS, nitric oxide synthase; L-NNA, *N*-nitro-L-arginine; L-NPA, *N*-propyl-L-arginine; SEITU, *S*-ethylisothiourea; SENPITU, *S*-ethyl-*N*-phenylisothiourea; H_4B, tetrahydrobiopterin.

References

(1) Groves, J. T.; Wang C. C. Nitric oxide synthase: Models and mechanisms. *Curr. Opin. Chem. Biol.* **2000**, *4*, 687−695.

(2) Alderton, W. K.; Cooper, C. E.; Knowles, R. G. Nitric oxide synthases: Structure, function and inhibition. *Biochem. J.* **2001**, *357*, 593−615.

(3) Kerwin, J. F., Jr.; Heller, M. The arginine−nitric oxide pathway: A target for new drugs. *Med. Res. Rev.* **1994**, *14*, 23−74.

(4) Nakane, M.; Schmidt, H. H.; Pollock, J. S.; Forstermann, U.; Murad F. Cloned human brain nitric oxide synthase is highly expressed in skeletal muscle. *FEBS Lett.* **1993**, *316*, 175−180.

(5) Bredt, D. S.; Hwang, P. M.; Glatt, C. E.; Lowenstein, C.; Reed, R. R.; Snyder, S. H. Cloned and expressed nitric oxide synthase structurally resembles cytochrome P-450 reductase. *Nature* **1991**, *351*, 714−718.

(6) Janssens, S. P.; Shimouchi, A.; Quertermous, T.; Bloch, D. B.; Bloch, K. D. Cloning and expression of a cDNA encoding human endothelium-derived relaxing factor/nitric oxide synthase. *J. Biol. Chem.* **1992**, *267*, 14519−14522.

(7) Lamas, S.; Marsden, P. A.; Li, G. K.; Tempst, P.; Michel, T. Endothelial nitric oxide synthase: Molecular cloning and characterization of a distinct constitutive enzyme isoform. *Proc. Natl. Acad. Sci. U.S.A.* **1992**, *89*, 6348−6352.

(8) Geller, D. A.; Lowenstein, C. J.; Shapiro, R. A.; Nussler, A. K.; Di Silvio, M.; Wang, S. C.; Nakayama, D. K.; Simmons, R. L.; Snyder, S. H.; Billiar, T. R. Molecular cloning and expression of inducible nitric oxide synthase from human hepatocytes. *Proc. Natl. Acad. Sci. U.S.A.* **1993**, *90*, 3491−3495.

(9) Xie, Q. W.; Cho, H. J.; Calaycay, J.; Mumford, R. A.; Swiderek, K. M.; Lee, T. D.; Ding, A.; Troso, T.; Nathan, C. Cloning and characterization of inducible nitric oxide synthase from mouse macrophages. *Science* **1992**, *256*, 225−228.

(10) Hobbs, A. J.; Higgs, A.; Moncada, S. Inhibition of nitric oxide synthase as a potential therapeutic target. *Annu. Rev. Pharmacol. Toxicol.* **1999**, *39*, 191−220.

(11) Aoyagi, M.; Arvai, A. S.; Tainer, J. A.; Getzoff, E. D. Structural basis for endothelial nitric oxide synthase binding to calmodulin. *EMBO J.* **2003**, *22*, 766−775.

(12) Roman, L. J.; Martasek, P.; Masters, B. S. Intrinsic and extrinsic modulation of nitric oxide synthase activity. *Chem. Rev.* **2002**, *102*, 1179−1190.

(13) Blasko, E.; Glaser, C. B.; Devlin, J. J.; Xia, W.; Feldman, R. I.; Polokoff, M. A.; Phillips, G. B.; Whitlow, M.; Auld, D. S.; McMillan, K.; Ghosh, S.; Stuehr, D. J.; Parkinson, J. F. Mechanistic studies with potent and selective inducible nitric-oxide synthase dimerization inhibitors. *J. Biol. Chem.* **2002**, *277*, 295−302.

(14) Wei, C.-C.; Wang, Z.-Q.; Arvai, A. S.; Hemann, C.; Hille, R.; Getzoff, E. D.; Stuehr, D. J. Structure of tetrahydrobiopterin tunes its electron transfer to the heme-dioxy intermediate in nitric oxide synthase. *Biochemistry* **2003**, *42*, 1969−1977.

(15) Kotsonis, P.; Frohlich, L. G.; Raman, C. S.; Li, H.; Berg, M.; Gerwig, R.; Groehn, V.; Kang, Y.; Al-Masoudi, N.; Taghavi-Moghadam, S.; Mohr, D.; Munch, U.; Schnabel, J.; Martasek, P.; Masters, B. S.; Strobel, H.; Poulos, T.; Matter, H.; Pfleiderer, W.; Schmidt, H. H. Structural basis for pterin antagonism in nitric-oxide synthase. Development of novel 4-oxo-pteridine antagonists of (6*R*)-5,6,7,8-tetrahydrobiopterin. *J. Biol. Chem.* **2001**, *276*, 49133−49141.

(16) Bredt, D. S.; Snyder, S. H. Isolation of nitric oxide synthetase, a calmodulin-requiring enzyme. *Proc. Natl. Acad. Sci. U.S.A.* **1990**, *87*, 682−685.

(17) Forstermann, U.; Pollock, J. S.; Schmidt, H. H.; Heller, M.; Murad, F. Calmodulin-dependent endothelium-derived relaxing factor/nitric oxide synthase activity is present in the particulate and cytosolic fractions of bovine aortic endothelial cells. *Proc. Natl. Acad. Sci. U.S.A.* **1991**, *88*, 1788−1792.

(18) Cho, H. J.; Xie, Q. W.; Calaycay, J.; Mumford, R. A.; Swiderek, K. M.; Lee, T. D.; Nathan, C. Calmodulin is a subunit of nitric oxide synthase from macrophages. *J. Exp. Med.* **1992**, *176*, 599−604.

(19) Huang, Z.; Huang, P. L.; Panahian, N.; Dalkara, T.; Fishman, M. C.; Moskowitz, M. A. Effects of cerebral ischemia in mice deficient in neuronal nitric oxide synthase. *Science* **1994**, *265*, 1883−1885.

(20) Huang, P. L.; Huang, Z.; Mashimo, H.; Bloch, K. D.; Moskowitz, M. A.; Bevan, J. A.; Fishman, M. C. Hypertension in mice lacking the gene for endothelial nitric oxide synthase. *Nature* **1995**, *377*, 239−242.

(21) Salerno, L.; Sorrenti, V.; Di Giacomo, C.; Romeo, G.; Siracusa, M. A. Progress in the development of selective nitric oxide synthase (NOS) inhibitors. *Curr. Pharm. Des.* **2002**, *8*, 177−200.

(22) Di Giacomo, C.; Sorrenti, V.; Salerno, L.; Cardile, V.; Guerrera, F.; Siracusa, M. A.; Avitabile, M.; Vanella, A. Novel Inhibitors of Neuronal Nitric Oxide Synthase. *Exp. Biol. Med.* **2003**, *228*, 486−490.

(23) Crane, B. R.; Arvai, A. S.; Gachhui, R.; Wu, C.; Ghosh, D. K.; Getzoff, E. D.; Stuehr, D. J.; Tainer, J. A. The structure of nitric oxide synthase oxygenase domain and inhibitor complexes. *Science* **1997**, *278*, 425−431.

(24) Crane, B. R.; Arvai, A. S.; Ghosh, D. K.; Wu, C.; Getzoff, E. D.; Stuehr, D. J.; Tainer, J. A. Structure of nitric oxide synthase oxygenase dimer with pterin and substrate. *Science* **1998**, *279*, 2121−2126.

(25) Raman, C. S.; Li, H.; Martasek, P.; Kral, V.; Masters, B. S.; Poulos, T. L. Crystal structure of constitutive endothelial nitric oxide synthase: A paradigm for pterin function involving a novel metal center. *Cell* **1998**, *95*, 939−950.

(26) Fischmann, T. O.; Hruza, A.; Niu, X. D.; Fossetta, J. D.; Lunn, C. A.; Dolphin, E.; Prongay, A. J.; Reichert, P.; Lundell, D. J.; Narula, S. K.; Weber, P. C. Structural characterization of nitric oxide synthase isoforms reveals striking active-site conservation. *Nat. Struct. Biol.* **1999**, *6*, 233−242.

(27) Li, H.; Raman, C. S.; Glaser, C. B.; Blasko, E.; Young, T. A.; Parkinson, J. F.; Whitlow, M.; Poulos, T. L. Crystal structures of zinc-free and -bound heme domain of human inducible nitric-oxide synthase. Implications for dimer stability and comparison with endothelial nitric-oxide synthase. *J. Biol. Chem.* **1999**, *274*, 21276−21284.

(28) Li, H.; Shimizu, H.; Flinspach, M.; Jamal, J.; Yang, W.; Xian, M.; Cai, T.; Wen, E. Z.; Jia, Q.; Wang, P. G.; Poulos, T. L. The novel binding mode of *N*-alkyl-*N*′-hydroxyguanidine to neuronal nitric oxide synthase provides mechanistic insights into NOS biosynthesis. *Biochemistry* **2002**, *41*, 13868−13875.

(29) Kastenholz, M. A.; Pastor, M.; Cruciani, G.; Haaksma, E. E.; Fox, T. GRID/CPCA: A new computational tool to design selective ligands. *J. Med. Chem.* **2000**, *43*, 3033−3044.

(30) Terp, G. E.; Cruciani, G.; Christensen, I. T.; Jorgensen, F. S. Structural differences of matrix metalloproteinases with potential implications for inhibitor selectivity examined by the GRID/CPCA approach. *J. Med. Chem.* **2002**, *45*, 2675−2684.

(31) Ridderstrom, M.; Zamora, I.; Fjellstrom, O.; Andersson, T. B. Analysis of selective regions in the active sites of human cytochromes P450, 2C8, 2C9, 2C18, and 2C19 homology models using GRID/CPCA. *J. Med. Chem.* **2001**, *44*, 4072−4081.

(32) Morris, G. M.; Goodsell, D. S.; Halliday, R. S.; Huey, R.; Hart, W. E.; Belew, R. K.; Olson, A. J. Automated docking using a Lamarckian genetic algorithm and an empirical binding free energy function. *J. Comput. Chem.* **1998**, *19*, 1639−1662.

(33) Raman, C. S.; Li, H.; Martasek, P.; Southan, G.; Masters, B. S.; Poulos, T. L. Crystal structure of nitric oxide synthase bound to nitro indazole reveals a novel inactivation mechanism. *Biochemistry* **2001**, *40*, 13448−13455.
(34) Raman, C. S.; Li, H.; Martasek, P.; Babu, B. R.; Griffith, O. W.; Masters, B. S.; Poulos, T. L. Implications for isoform-selective inhibitor design derived from the binding mode of bulky isothioureas to the heme domain of endothelial nitric-oxide synthase. *J. Biol. Chem.* **2001**, *276*, 26486−26491.
(35) Crane, B. R.; Arvai, A. S.; Ghosh, S.; Getzoff, E. D.; Stuehr, D. J.; Tainer, J. A. Structures of the N^{ω}-hydroxy-L-arginine complex of inducible nitric oxide synthase oxygenase dimer with active and inactive pterins. *Biochemistry* **2000**, *39*, 4608−4621.
(36) *SYBYL Molecular Modelling Package*, version 6.8; Tripos, St. Louis, MO, 2001.
(37) *GRID*, version 20; Molecular Discovery Ltd., 4 Chandos street, London, U.K., 2002.
(38) *GOLPE4.5*. Multivariate Informetric Analysis Srl., Viale dei Castagni 16, Perugia Italy, 1999.
(39) Westerhuis, J. A.; Kourti, T.; Macgregor, J. F. Analysis of multiblock and hierarchical PCA and PLS models. *J. Chemom.* **1998**, *12*, 301−321.
(40) Weiner, S. J.; Kollman, P. A.; Case, D. A.; Singh, U. C.; Ghio, C.; Alagona, G.; Profeta, S.; Weiner, P. A new force field for molecular mechanical simulation of nucleic acid and proteins. *J. Am. Chem. Soc.* **1984**, *106*, 765−784.
(41) Gasteiger, J.; Marsili, M. Iterative paratial equalization of orbital electronegativity−a rapid access to atomic charges. *Tetrahedron* **1980**, *36*, 3219−3228.
(42) Morris, G. M.; Goodsell, D. S.; Huey, R.; Olson, A. J. Distributed automated docking of flexible ligands to proteins: Parallel applications of AutoDock 2.4. *J. Comput.-aided Mol. Des.* **1996**, *10*, 293−304.
(43) Hetenyi, C.; Van Der Spoel, D. Efficient docking of peptides to proteins without prior knowledge of the binding site. *Protein Sci.* **2002**, *11*, 1729−1737.
(44) Babu, B. R.; Frey, C.; Griffith, O. W. L-arginine binding to nitric-oxide synthase. The role of H-bonds to the nonreactive guanidinium nitrogens. *J. Biol. Chem.* **1999**, *274*, 25218−25226.
(45) Li, H.; Raman, C. S.; Martasek, P.; Kral, V.; Masters, B. S. S.; Poulos, T. L. Mapping the active site polarity in structures of endothelial nitric oxide synthase heme domain complexed with isothioureas. *J. Inorg. Biochem.* **2000**, *81*, 133−139.
(46) Babu, B. R.; Griffith, O. W. N^5-(1-Imino-3-butenyl)-L-ornithine. A neuronal isoform selective mechanism-based inactivator of nitric oxide synthase. *J. Biol. Chem.* **1998**, *273*, 8882−8889.
(47) Furfine, E. S.; Harmon, M. F.; Paith, J. E.; Garvey, E. P. Selective inhibition of constitutive nitric oxide synthase by L-N^G-nitroarginine. *Biochemistry* **1993**, *32*, 8512−8517.
(48) Zhang, H. Q.; Fast, W.; Marletta, M. A.; Martasek, P.; Silverman, R. B. Potent and selective inhibition of neuronal nitric oxide synthase by N^{ω}-propyl-L-arginine. *J. Med. Chem.* **1997**, *40*, 3869−3870.
(49) Matter, H.; Kotsonis, P.; Klingler, O.; Strobel, H.; Frohlich, L. G.; Frey, A.; Pfleiderer, W.; Schmidt, H. H. Structural requirements for inhibition of the neuronal nitric oxide synthase (NOS-I): 3D-QSAR analysis of 4-oxo- and 4-amino-pteridine-based inhibitors. *J. Med. Chem.* **2002**, *45*, 2923−2941.
(50) Silverman, R. B.; Huang, H.; Marletta, M. A.; Martasek, P. Selective inhibition of neuronal nitric oxide synthase by N omega-nitroarginine-and phenylalanine-containing dipeptides and dipeptide esters. *J. Med. Chem.* **1997**, *40*, 2813−2817.
(51) Huang, H.; Martasek, P.; Roman, L. J.; Masters, B. S.; Silverman, R. B. N^{ω}-Nitroarginine-containing dipeptide amides. Potent and highly selective inhibitors of neuronal nitric oxide synthase. *J. Med. Chem.* **1999**, *42*, 3147−3153.
(52) Huang, H.; Martasek, P.; Roman, L. J.; Silverman, R. B. Synthesis and evaluation of peptidomimetics as selective inhibitors and active site probes of nitric oxide synthases. *J. Med. Chem.* **2000**, *43*, 2938−2945.
(53) Huang, H.; Martasek, P.; Roman, L. J.; Silverman, R. B. Synthesis and evaluation of dipeptide amides containing N^{ω}-nitroarginine and D-2,4-diaminobutyric acids as inhibitors of neuronal nitric oxide synthase. *J. Enzyme Inhib.* **2001**, *16*, 233−239.
(54) Hah, J. M.; Roman, L. J.; Martasek, P.; Silverman, R. B. Reduced amide bond peptidomimetics. (4*S*)-*N*-(4-amino-5-[aminoakyl]-aminopentyl)-*N*′-nitroguanidines, potent and highly selective inhibitors of neuronal nitric oxide synthase. *J. Med. Chem.* **2001**, *44*, 2667−2670.
(55) Hah, J.-M.; Martasek, P.; Roman, L. J.; Silverman, R. B. Aromatic Reduced Amide Bond Peptidomimetics as Selective Inhibitors of Neuronal Nitric Oxide Synthase. *J. Med. Chem.* **2003**, *46*, 1661−1669.
(56) Chabrier, P. E.; Auguet, M.; Spinnewyn, B.; Auvin, S.; Cornet, S.; Demerle-Pallardy, C.; Guilmard-Favre, C.; Marin, J. G.; Pignol, B.; Gillard-Roubert, V.; Roussillot-Charnet, C.; Schulz, J.; Viossat, I.; Bigg, D.; Moncada, S. BN 80933, a dual inhibitor of neuronal nitric oxide synthase and lipid peroxidation: A promising neuroprotective strategy. *Proc. Natl. Acad. Sci. U.S.A.* **1999**, *96*, 10824−10829.
(57) Hagen, T. J.; Bergmanis, A. A.; Kramer, S. W.; Fok, K. F.; Schmelzer, A. E.; Pitzele, B. S.; Swenton, L.; Jerome, G. M.; Kornmeier, C. M.; Moore, W. M.; Branson, L. F.; Connor, J. R.; Manning, P. T.; Currie, M. G.; Hallinan, E. A. 2-Iminopyrrolidines as potent and selective inhibitors of human inducible nitric oxide synthase. *J. Med. Chem.* **1998**, *41*, 3675−3683.
(58) Flinspach, M. L.; Li, H.; Jamal, J.; Yang, W.; Huang, H.; Hah, J.-M.; Gomez-Vidal, J. A.; Litzinger, E. A.; Silverman, R. B.; Poulos, T. L. Structure basis for dipeptide amide isoform-selective inhibition of neuronal nitric oxide synthase. *Nat. Struct. Biol.* **2003**, *10*, in press.
(59) Zhang, H. Q.; Dixon, R. P.; Marletta, M. A.; Nikolic, D.; Van Breemen, R.; Silverman R. B. Mechanism of inactivation of neuronal nitric oxide synthase by N^{ω}-Allyl-L-arginine. *J. Am. Chem. Soc.* **1997**, *119*, 10888−10902.
(60) Cooper G. R.; Mialkowski K.; Wolff D. J. Cellular and enzymatic studies of N^{ω}-propyl-L-arginine and *S*-ethyl-*N*-[4-(trifluoromethyl)phenyl]isothiourea as reversible, slowly dissociating inhibitors selective for the neuronal nitric oxide synthase isoform. *Arch. Biochem. Biophys.* **2000**, *375*, 183−194.

JM030301U